Hindawi
Geofluids
Volume 2022, Article ID 3463752, 15 pages
https://doi.org/10.1155/2022/3463752

Research Article

Research on the Influence of Groundwater in Coastal Areas on the Stress and Deformation Characteristics of Integrated Pipe Gallery

Yuanyuan Tian,[1] Qingbiao Wang,[2,3,4] Zhongjing Hu,[2] Shuo Yang,[1] Chuanxiong Peng,[3] Xu Zhang,[5] Zhongying Li,[6] and Xugang Wang[7]

[1]*College of Civil Engineering and Architecture, Shandong University of Science and Technology, Qingdao 266590, China*
[2]*College of Safety and Environmental Engineering (College of Safety and Emergency Management), Shandong University of Science and Technology, Qingdao 266590, China*
[3]*College of Resources, Shandong University of Science and Technology, Taian 271000, China*
[4]*National Engineering Laboratory for Coalmine Backfilling Mining, Shandong University of Science and Technology, Taian 271019, China*
[5]*Shandong Transportation Research Institute, Jinan 250102, China*
[6]*School of Civil and Resource Engineering, University of Science and Technology Beijing, Beijing 100083, China*
[7]*Beijing Anjie Engineering Consulting Co., Ltd., Beijing 100051, China*

Correspondence should be addressed to Zhongjing Hu; huyang@sdust.edu.cn

Received 8 July 2022; Accepted 29 August 2022; Published 17 September 2022

Academic Editor: Zhengzheng Xie

With the high demand for basic resources such as electricity, communication, water supply, and gas in cities, most cities in my country are vigorously developing underground integrated pipe gallery. When constructing pipe gallery in coastal areas, it is necessary to consider the impact of groundwater level on structural calculations. There is still a lack of systematic research in domestic and foreign literature. Relying on the Qingdao West Coast New Area Project, this paper uses a combination of laboratory tests and MIDAS GTS/NX numerical simulation to study the influence of groundwater in the coastal area on the stress and deformation characteristics of the integrated pipe gallery. The results show that (1) the Mises stress on the roof and bottom of the integrated pipe gallery increases continuously with the rise of the groundwater level. Due to the effect of the effective stress, the Mises stress on the side wall shows a decreasing trend. (2) Due to the influence of the construction form of the cross-section interface, the maximum principal stress of each part of the *M* side is always smaller than that of the *N* side; with the continuous increase of groundwater level, the maximum principal stress at each part of the *N* and *M* sides of the pipe gallery structure joint gradually increases. (3) The overall structure of the pipe gallery floats up. Under the action of the buoyancy force, the bottom plate moves upward, and the surface displacement rises continuously with the rise of the groundwater level. (4) When the groundwater depth is the same, the analysis of the test results and the numerical simulation calculation results are basically consistent, which further verifies the validity of the numerical simulation calculation and has reference value. (5) The engineering example shows that in order to reduce the service life of the integrated pipe gallery, the impact of groundwater on the integrated pipe gallery cannot be ignored.

1. Introduction

Since the groundwater level is not constant, it changes with the change of the external environment. When the prefabricated integrated pipe gallery is buried underground and is located in the urban water-rich area, the groundwater level will be caused by surface precipitation, climate change, and seaside tidal effects. In addition, the pipe gallery will be affected by

the buoyancy of groundwater as the groundwater level rises, causing hidden dangers for the stability of the pipe gallery structure and safe operation, which will inevitably affect the stress deformation of the integrated pipe gallery and the interaction between the structure and the soil. Groundwater is an important factor affecting the structure of underground pipe gallery; so, it is very necessary to study the influence of groundwater on integrated pipe gallery in coastal areas.

Wang et al. [1] studied the effect of groundwater level on the stability of shallow tunnels, and the results showed that the extent of roof collapse increases when the groundwater level drops. Wu et al. [2] analyzed the relationship between land subsidence, tunnel deformation, and water level changes, and the results showed that the groundwater level changes caused by tides will directly affect the floating or subsidence of shield tunnels. Tang et al. [3] discussed the relationship between surface subsidence and pore pressure changes, and the results showed that consolidation caused by high pore pressure changes is considered to be the main mechanism of surface subsidence. Shin et al. [4] studied the effect of groundwater flow on a deep circular tunnel with an elastic-plastic homogeneous foundation, and the results showed that groundwater flow at the tunnel wall affects radial and axial deformations. Xu and Li [5] studied the effect of continuous rainfall on the stability of shallow weathered rock tunnels. The results show that the infiltration of rainwater makes the surrounding rock of shallow weathered rock tunnels soften continuously due to continuous rainfall, resulting in the stiffness and confining pressure of surrounding rock coefficient decreases. Bhattacharya and Dutta [6] found that in the process of tunneling in the presence of groundwater table, seepage force will be generated, which will lead to the decrease of rock mass stability. The results of Li et al. [7] indicated that the dynamic characteristics of regional groundwater and the temporal and spatial evolution of seepage field under the influence of tides must be considered in engineering construction. The results of Deng et al. [8] showed that when excavating tunnels in water-rich soft rock formations, the infiltration of groundwater greatly reduced the strength of the soft rock. The results of Wang et al. [9] show that the influence of groundwater on tunnel engineering is very complex. The surrounding rock has the characteristics of dynamic pressure arch during the seepage failure process, but collapse failure is more likely to occur under low water pressure. The results of Wei and Zhu [10] concluded that grouting reinforcement can effectively block groundwater seepage. The results of Guo et al. [11] show that the groundwater level has the characteristics of periodic fluctuation with the tide. The results of Hu et al. [12] show that considering the influence of the seepage of soft soil foundation, the maximum vertical displacement of the ground surface in each excavation stage occurs near the underground diaphragm wall. Gia et al. [13] studied the effect of groundwater table reduction on the bearing capacity of pile foundations. Roh et al. [14] analyzed the load-settlement curve of pile-raft foundation and the variation law of axial bearing capacity with groundwater level based on finite element analysis. Saowiang and Giao [15] studied the effect of pore pressure and undrained shear strength variation of the clay layer on ultimate pile bearing capacity. Shi et al. [16] considered the influence of groundwater seepage force and analyzed the working face stability of underwater tunnels constructed by the fracture zone mining method based on numerical simulation. Zhang et al. [17] showed that reservoir cisterns located near tunnel structures have negative effects on groundwater seepage to varying degrees. Ding et al. [18] investigated the effect of groundwater level on the seismic response of coral sand foundation-superstructure systems through a series of shaking table experiments. Ratnika et al. [19] studied the effect of groundwater level changes on the modal parameters of mid-rise and high-rise reinforced concrete buildings and found that the rise in groundwater level resulted in a decrease in natural frequency values. Shi et al. [20] studied the deformation process and influencing factors of the drainage excavation of the deep foundation pit of the station and analyzed the influence of different predewatering conditions and the depth of the water stop on the deformation of the foundation pit. Wu et al. [21] used wavelet coherence to analyze the relationship between groundwater level and lake level, and the results showed that the groundwater level in the lakeshore area was positively correlated with the lake level during a short lag period of about 30 days. Zeng et al. [22] stated that using two methods of field pumping test and numerical simulation, the influence mechanism of precipitation in the foundation pit and the deflection of the retaining wall on the ground subsidence outside the foundation pit was studied, and the characteristics of surface subsidence under the combined action of groundwater subsidence and wall movement were revealed. Zaryab et al. [23] showed that rapid urbanization has had a serious adverse impact on both the quantity and quality of groundwater. The results of Zhou et al. [24] showed that the impact of climate change on the groundwater level in the regional groundwater system has obvious spatial variability. Liu et al. [25] studied the effects of different zonal coastline types on the groundwater level of coastal wetlands in the Yellow River Delta in China. Yan et al. [26] used a nonparametric statistical test method to study the variation trend of groundwater table depth. Guo et al. [27] studied the effect of groundwater level changes on the frost heave deformation of the foundation soil, the bending moment of the channel section, and the migration of the water content of the foundation.

The research method of similar model test has been deeply explored by many scholars in different academic fields. The research results of Chen et al. [28–30] show that the physical model of geotechnical engineering can accurately simulate the characteristics of the prototype on the basis of satisfying the similarity principle and achieved good experimental results. Shi et al. [31] used a similar model test to discuss the deformation and fracture mechanism of the floor of the long-span coal mining chamber in a deep mine and verified the reliability of the theoretical analysis. Chai et al. [32] confirmed that physical similarity model checking is one of the main research methods for mining engineering problems. Jiang et al. [33] designed and produced two physical test models with a ratio of 1 : 10 based on similarity theory. Zhao et al. [34] introduced the data collection elements and various monitoring methods of model tests and studied the rationality of similar material test techniques. Chen and Ren [35] developed a new type of similar material based on the similarity theory of geomechanical model tests. Zhao and He [36] established a three-dimensional physical model based on

similarity theory and met the similarity requirements of physical and mechanical properties such as elastic modulus, compressive strength, and Poisson's ratio. Dong et al. [37] established a risk control method to ensure the construction safety of comprehensive underground pipe gallery in complex surrounding environment. The numerical results of Zhao et al. [38] show that reducing the crankshaft speed and increasing the intake pressure will reduce the backflow of external air from the pore boundary and increase the oil injection rate, and the proposed numerical model can predict the complex two-phase flow phenomenon in the channel.

To sum up, many scholars have studied more about the influence of groundwater on shallow tunnels, and some scholars have studied the influencing factors and prediction methods of groundwater level changes. At present, the relevant documents issued by the state have indicated that it is necessary to vigorously develop the underground integrated pipe gallery project. Since the pipe gallery structure is shallowly buried in the soil below the pavement of the carriageway, there is a lack of systematic research on the mechanical characteristics of the pipe gallery under the condition of water level changes. It is difficult to ensure the accuracy of the study by using similar data conclusions for the stress and deformation characteristics of underground structures with different engineering properties. Therefore, exploring the stress and deformation of urban integrated pipe gallery caused by groundwater changes is conducive to targeted protection of pipe gallery structure and reasonable design of waterproof measures.

Based on the Lingshan Bay Road integrated pipe gallery project in the West Coast New Area of Qingdao, this paper adopts the method of combining similar model experiments and MIDAS GTS/NX software numerical simulation to study the stress deformation and surface displacement of the integrated pipe gallery under different water levels of the groundwater in the coastal area.

2. Engineering Background

The integrated pipe gallery project of Lingshan Bay Road is located in the southwestern part of Qingdao City, China, with a total length of 4065 m, of which the prefabricated section is about 2300 m. The single cabin structure section is adopted, and the net section size is $B * H = 3\,\text{m} * 3\,\text{m}$. The structural form is reinforced concrete rectangular frame. The length of the prefabricated pipe section is 1.5 m, and the wall thickness is 0.3 m. The joint is designed by the socket, and the open excavation method is used. The location map of the Qingdao project is shown in Figure 1.

3. Experiment and Analysis of Experimental Results

3.1. Determination of Similarity Relationship. The model experiment material studied is derived from the basic principles of elasticity and rock mechanics, that is, the model material should conform to Hooke's theorem as the prototype, and all points in the model should satisfy the equilibrium equation, compatibility equation, and geometric

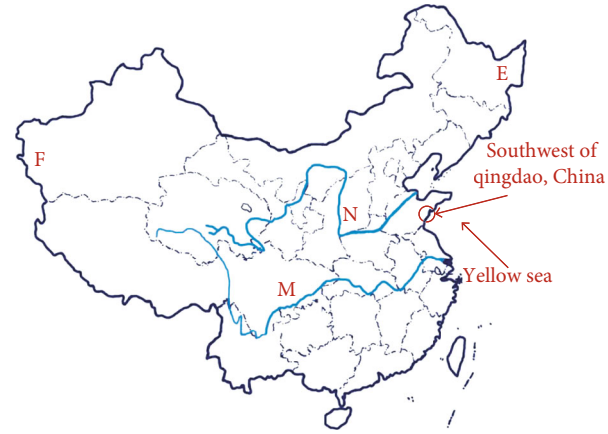

Figure 1: Location map of Qingdao engineering projects.

Table 1: The similarity ratio relationship of each index in the experiment.

Physical quantity	C_l	C_σ	C_δ	C_ρ	C_E	C_μ	C_c	C_γ	C_f	C_F
Similar ratio	7.5	7.5	7.5	1	7.5	1	7.5	1	1	7.5^3

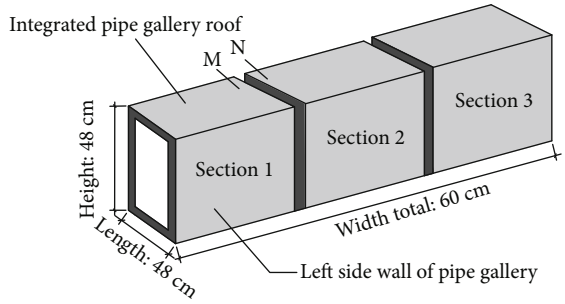

Figure 2: Elevation view of prefabricated pipe gallery.

equation. All points on the surface should satisfy the boundary conditions [28–33].

The ratio of the same physical quantity between the prototype (p) and the model (m) is called the similarity scale and is replaced by the letter C. Therefore, the similarity scale should satisfy the following relationship:

(1) The relationship between C_σ, C_r, and C_l is $C_\sigma = C_\gamma C_l$

(2) The relationship between C_σ, C_E, and C_ε is $C_\sigma = C_\varepsilon C_E$

(3) The relationship between C_δ, C_l, and C_ε is $C_\delta = C_\varepsilon C_l$

(4) The similarity scale of all dimensionless physical quantities in the prototype and the model is equal to 1, and the similarity scales of the same dimensional physical quantities are equal, namely,

$$C_\varepsilon = 1, C_f = 1, C_\varphi = 1, C_\mu = 1, \tag{1}$$

$$C_\sigma = C_E = C_c = C_{\sigma_c} = C_{\sigma_t}. \tag{2}$$

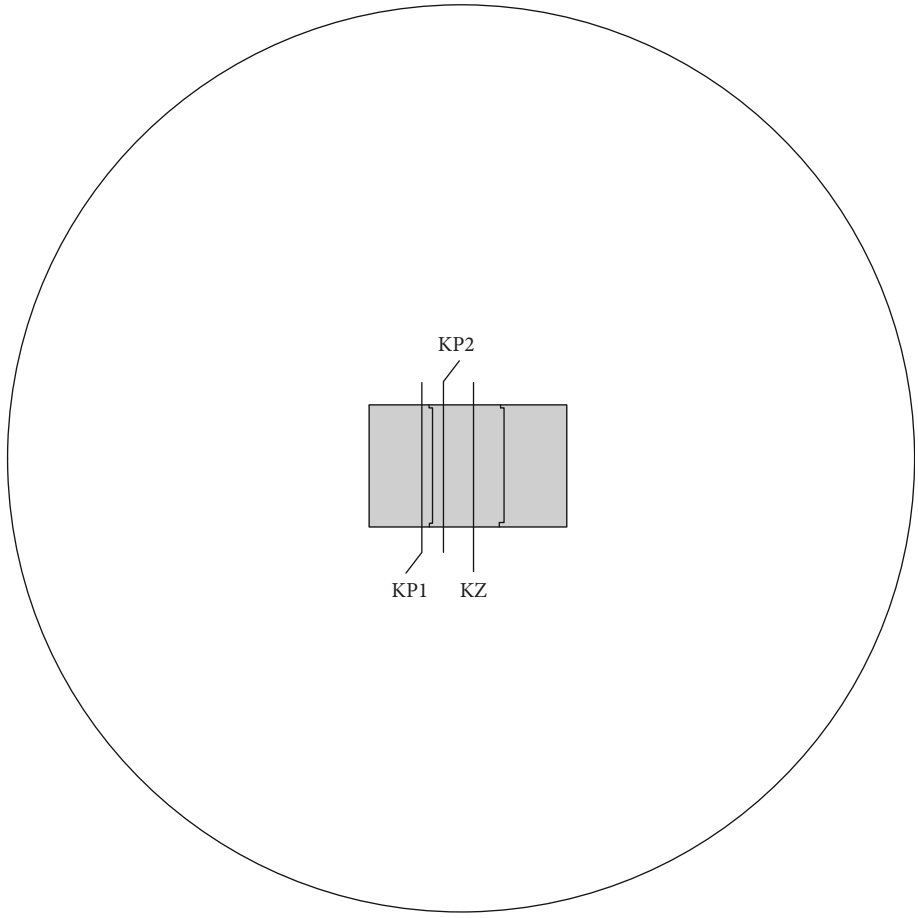

Figure 3: Monitoring point section position.

In the formula, l is the geometric length, δ is the displacement, σ is the stress, ε is the strain, F is the force, μ is Poisson's ratio, σ_t is the tensile strength, σ_c is the compressive strength, E is the elastic modulus, c is the adhesive force, γ is the bulk density, φ is the friction angle, and f is the friction coefficient. The similarity ratio of each index in the experiment is shown in Table 1.

3.2. Monitoring Point Layout

3.2.1. Section Selection. There are three sections of the integrated pipe gallery, and the experimental sections are selected as $J_{1-2}M$ side, $J_{2-1}N$ side end, and P2 mid-span. The meaning of J_{1-2} is the combination of the adjacent Section 1 and Section 2 of the integrated pipe gallery. For the joint section, Pi means the integrated pipe gallery of section i, and the three measurement sections are numbered as KP1 section, KP2 section, and KZ section. The elevation of the prefabricated pipe gallery is shown in Figure 2, and the selection of the longitudinal section of the measuring point is shown in Figure 3.

3.2.2. Layout of Stress Measuring Points. The stress measuring points are arranged around the inner wall of the integrated pipe gallery, and the selected sections in the experiment are arranged in the middle of the roof of the pipe section, the middle of the left and right side walls, the nodes of the roof and side walls on both sides, the middle of the floor, and the nodes of the floor and side walls on both sides. Eight measuring points are set for each section and numbered from the left armpit angle of the roof in clockwise direction, with a total of 24 stress measuring points. The number 2 represents the stress value at the mid-span of the roof plate, the number 3 represents the stress value at the right haunch corner of the roof plate, and the number 4 represents the stress value in the middle of the right side wall. The layout of the transverse section of the stress measuring points is shown in Figure 4.

3.2.3. Layout of Water Level and Surface Displacement Monitoring Points. The actual survey period of the project is the wet season, and the actual measurement of the water level of the borehole was carried out in the field. The buried depth of the stable water level is 1.00~2.70 m, and the elevation of the stable water level is 1.13~14.30 m. According to the regional hydrogeological data, the groundwater level the annual change range is about 1.50 m. The selection of the buried depth of the groundwater level not only considers the stable water level buried depth but also combines the four situations of the influence of the actual water level buried depth change on the structure of the integrated pipe gallery. The relationship between the groundwater level and the buried depth of the pipe gallery is shown in Figure 5.

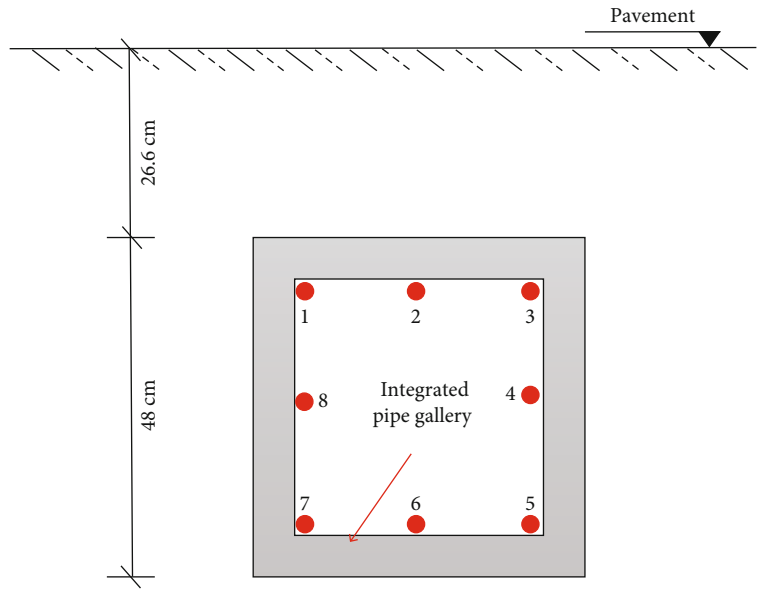

Figure 4: Layout of the transverse section of stress measuring points.

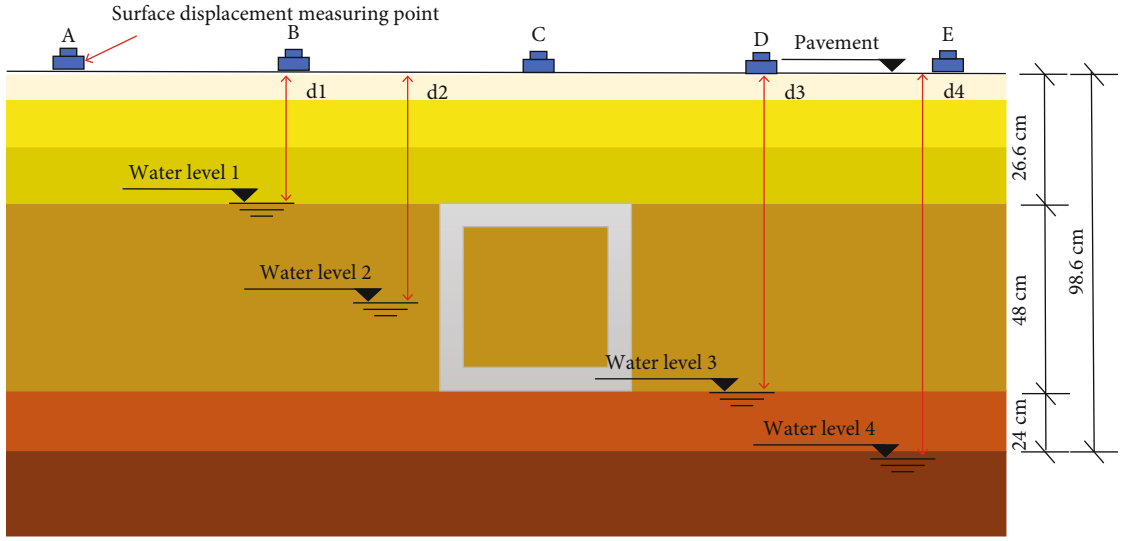

Figure 5: The relationship between groundwater level and buried depth of pipe gallery.

There are 5 monitoring points of surface displacement. The relationship between the groundwater level and the buried depth of the pipe gallery is as follows: from the initial water level (water level 4) to the bottom plate position (water level 3) from 1.8 m below the bottom plate of the integrated pipe gallery, when it rises 1.8 m above the bottom plate (water level 2), and when it rises to the top plate position (water level 1), AND the stress and deformation law of the prefabricated integrated pipe gallery structure under different groundwater levels in the coastal area is analyzed. In Figure 5, d represents the height of the groundwater level from the surface, where d1 = 26.6 cm, d2 = 50.6 cm, d3 = 74.6 cm, and d4 = 98.6 cm.

The experiment only explores the stress change of each measuring point of the pipe gallery when the groundwater level is d2 and uses high-precision resistance strain gauges to collect the stress parameters of the structure (see Figure 6(a)), the model box (see Figure 6(c)) is a steel plate with a thickness of 5 mm, the upper opening is convenient for test operation, and the DHDAS dynamic signal acquisition system is used for data measurement.

3.3. Analysis of Experimental Data. According to the similarity ratio and similarity relationship, the calculation results of model test are converted into the analysis of prototype structure results. Due to the large amount of data collection during the experiment, the data stored by the computer after each loading is about 3000~5000, and the interference factors are inevitable in the test process. Therefore, after preprocessing the experimental data, the stress curve method is used to analyze the influence of vehicle loading on the pipe gallery under different working conditions. The structure is in the elastic

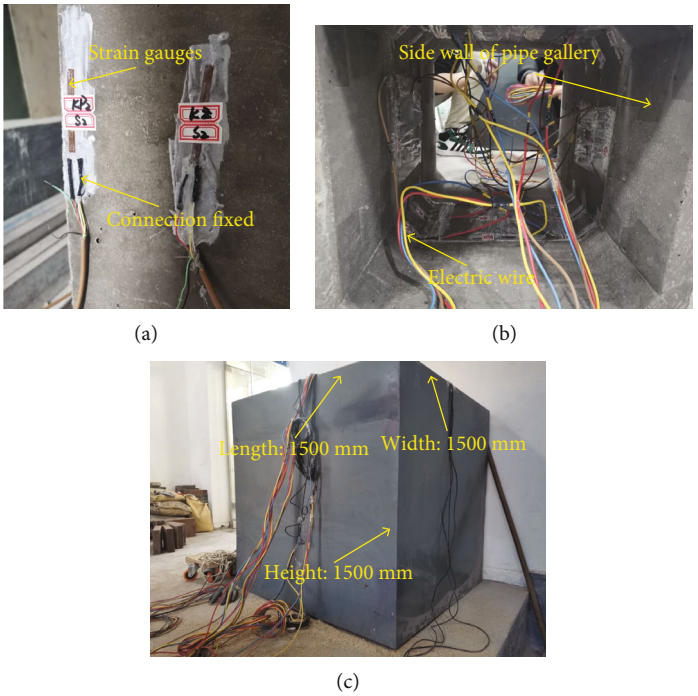

Figure 6: Laboratory apparatus. (a) Strain gauge. (b) Outer lead of the tube section. (c) Physical drawing of experimental model box.

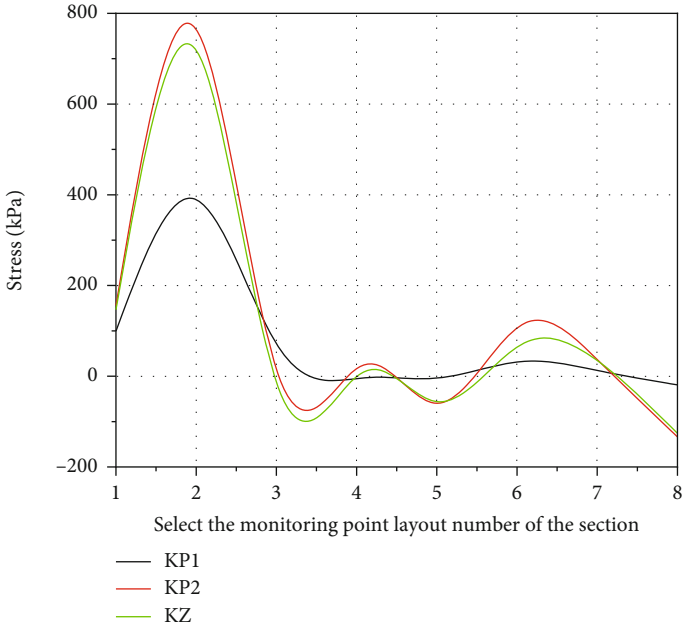

Figure 7: Stress distribution curve of each measuring point of the section.

deformation stage after loading. According to the linear proportional relationship in Hooke's law, the conversion formula between strain and stress is obtained: $\varepsilon \times E = \sigma$.

It can be seen from Figure 7 that the overall stress variation trends of KP1, KP2, and P2 mid-span sections are basically the same, and the maximum tensile stress is also in the mid-span of the roof. The stress of the roof and floor of the pipe gallery is backward concave to the inside, and the stress of the walls on both sides of the pipe gallery is backward convex. Under the same groundwater level, the stress of the KP2 section is the largest, followed by P2 span, and the stress of the KP1 section is the smallest.

Comparing the stress distribution curves of KP1 and KP2 section measuring points, it can be seen that the stress value of KP2 section measuring point is much larger than that of the KP1 section. Except for measuring point S2, the stress change range of KP2 section measuring point is larger than that of KP1 section measuring point. This may be related to the

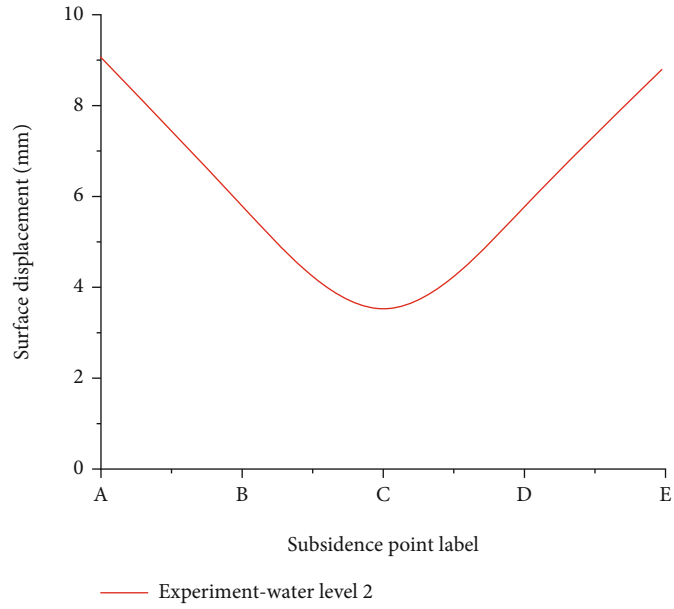

Figure 8: Surface displacement change map.

Table 2: Parameters of concrete plastic damage model.

Concrete grade	Density/kg.m^{-3}	Expansion angle	Offset value/m	f_{b0}/f_{c0}	K_c	Viscosity coefficient/μ
C40	25000	30°	0.1	1.16	0.667	0.0005

Table 3: Road and soil structure material parameters.

Material	Thickness/cm	E/MPa	μ	c/kPa	φ/°
Asphalt concrete	10	1250	0.3	/	/
ATB-30	12	1000	0.3	/	/
Cement stabilized crushed stone	36	1500	0.25	/	/
Lime soil	20	450	0.35	/	/
Silty clay	1200	5	0.35	31	12
Muddy silty clay	5000	3	0.4	15	8
Silty clay	1000	8	0.3	31	15
Coarse sand	3500	15	0.25	1	30
Strongly weathered granite	3500	20	0.3	50	35

design of the socket at the joint of two sections. It is difficult to ensure the tightness of the socket during the experiment.

As shown in Figure 8, when the groundwater level is d2, the overall structure of the pipe gallery floats up, and the bottom plate moves upward due to the action of the buoyancy force. Therefore, the displacement value becomes smaller, and the rising amplitude becomes smaller. The peak surface displacement changes are 6.22 mm, 5.18 mm, 3.21 mm, 5.09 mm, and 6.25 mm, respectively.

4. Numerical Simulation and Analysis of Simulation Results

4.1. Model Parameters. The MIDAS GTS/NX software was used to establish a three-dimensional solid pipe gallery model. The N and M sides of the joint were meshed, and the unilateral sockets were established at both ends of the overall model. The prestressed tendons with 100 kN pretension were applied at the four corners of the pipe gallery. The prefabricated pipe gallery has three sections with a total length of 4.5 m. The linear elastic model was used to simulate the concrete structure of the pipe gallery. The calculation parameters are C40 concrete parameters (shown in Table 2), elastic modulus 32.5 GPa, and Poisson's ratio 0.2.

A three-dimensional soil model is established according to the construction site stratum conditions and road parameters (as shown in Table 3). In order to reduce the influence of boundary effect, the stratum modeling size is selected according to the basic requirements of the model establishment in

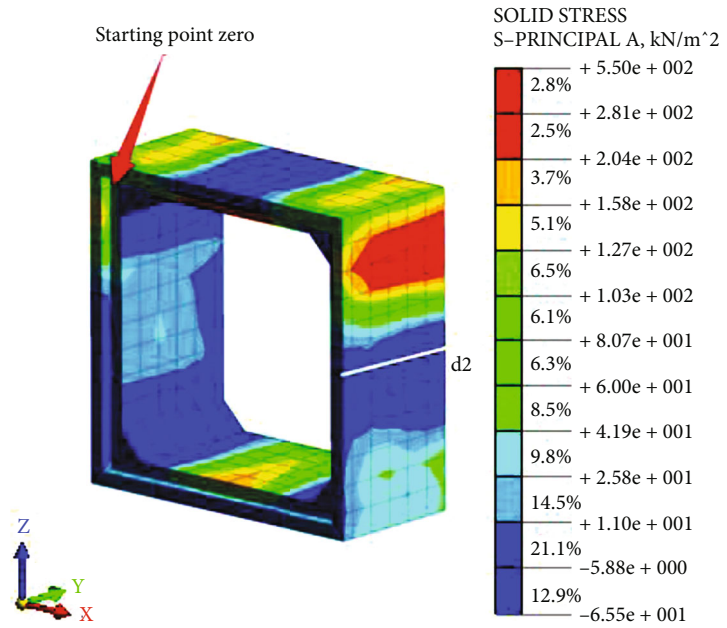

Figure 9: Contour map of the maximum principal stress on the *N* side.

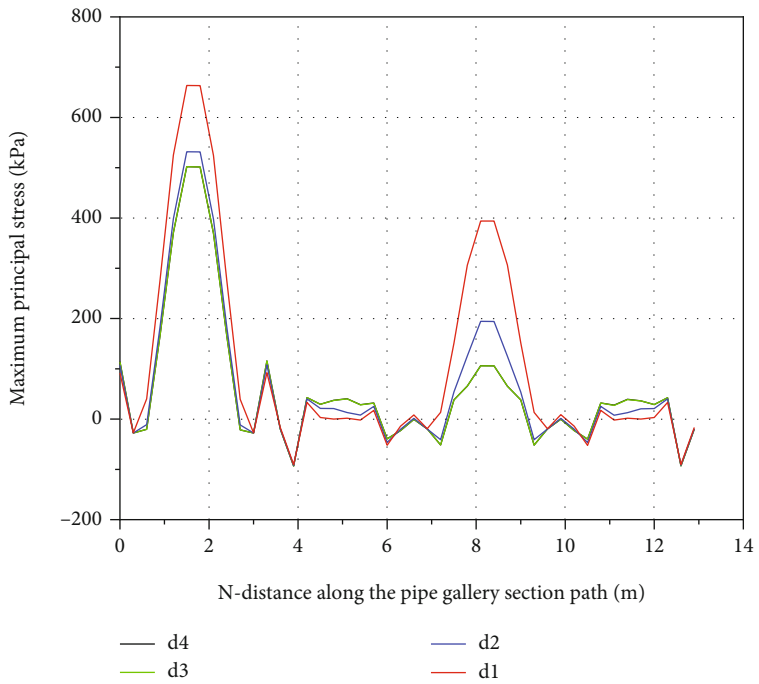

Figure 10: Distribution curve of maximum principal stress on the *N* side.

numerical simulation: longitudinal ∗ transverse ∗ height = 4.8 m ∗ 30 m ∗ 15 m. The linear elastic constitutive model is used for calculation, and the elastoplastic constitutive model can be used for filling and subgrade materials.

4.2. Simulation Data Analysis

4.2.1. Force Analysis of the Cross-Section of the N and M Sides at the Joints of the Integrated Pipe Gallery. According to Figures 9–12, in the change trend of the maximum principal stress of the tensile stress on the *N* and *M* sides at the joint along the section path of the pipe gallery, the maximum principal stress increases rapidly from the left side of the roof to the mid-span peak of the roof, then the tensile stress is rapidly decreasing, the minimum tensile stress appears at the right side haunch corner of the roof, the variation of the tensile stress of the left and right side walls is roughly symmetrical about the mid-span of the bottom plate, and the change value is always smaller than the tensile stress value of the bottom plate. The change trend is consistent

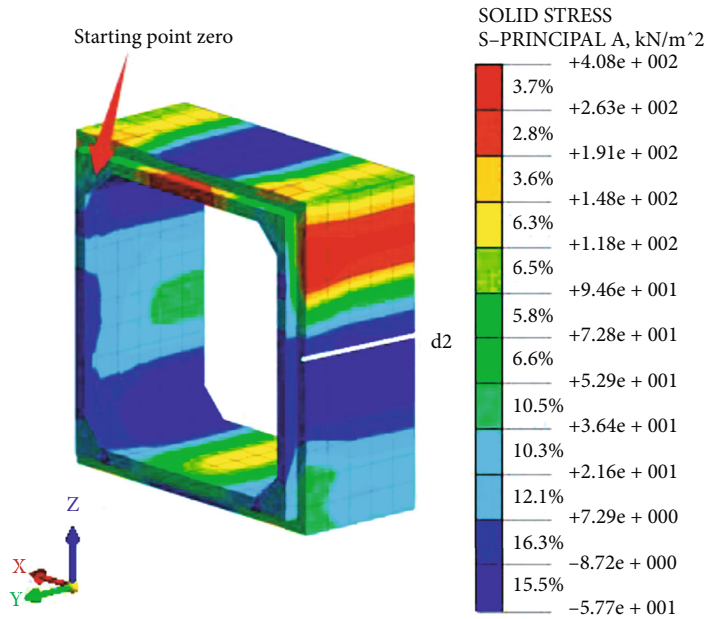

Figure 11: Contour map of maximum principal stress on the *M* side.

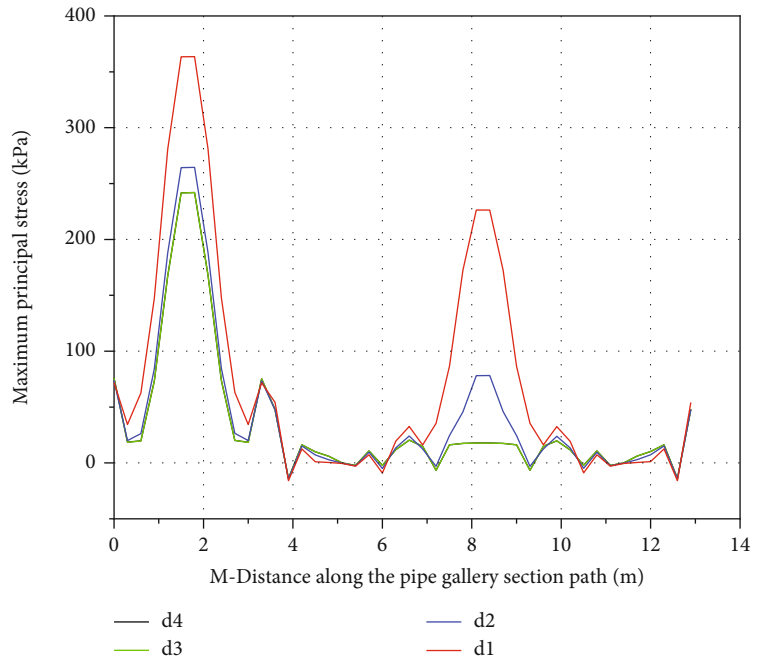

Figure 12: Distribution curve of maximum principal stress on the *M* side.

with the experimental analysis results and has reference value.

As the groundwater level rises, the maximum principal stress peaks on the *N* side of the pipe gallery are 502.01 kPa, 501.91 kPa, 531.68 kPa, and 663.70 kPa, and the maximum principal stress peaks on the *M* side of the pipe gallery are 242.03 kPa, 241.96 kPa, 264.52 kPa, and 363.60 kPa. Due to the influence of the structural form of the cross-section interface, the maximum principal stress value of each part of the *M* side is smaller than that of the *N* side.

In short, with the continuous rise of the groundwater level, the maximum principal stress of each part on the *N* and *M* sides of the joints of the pipe gallery structure shows a gradually increasing trend. The walls have not changed much.

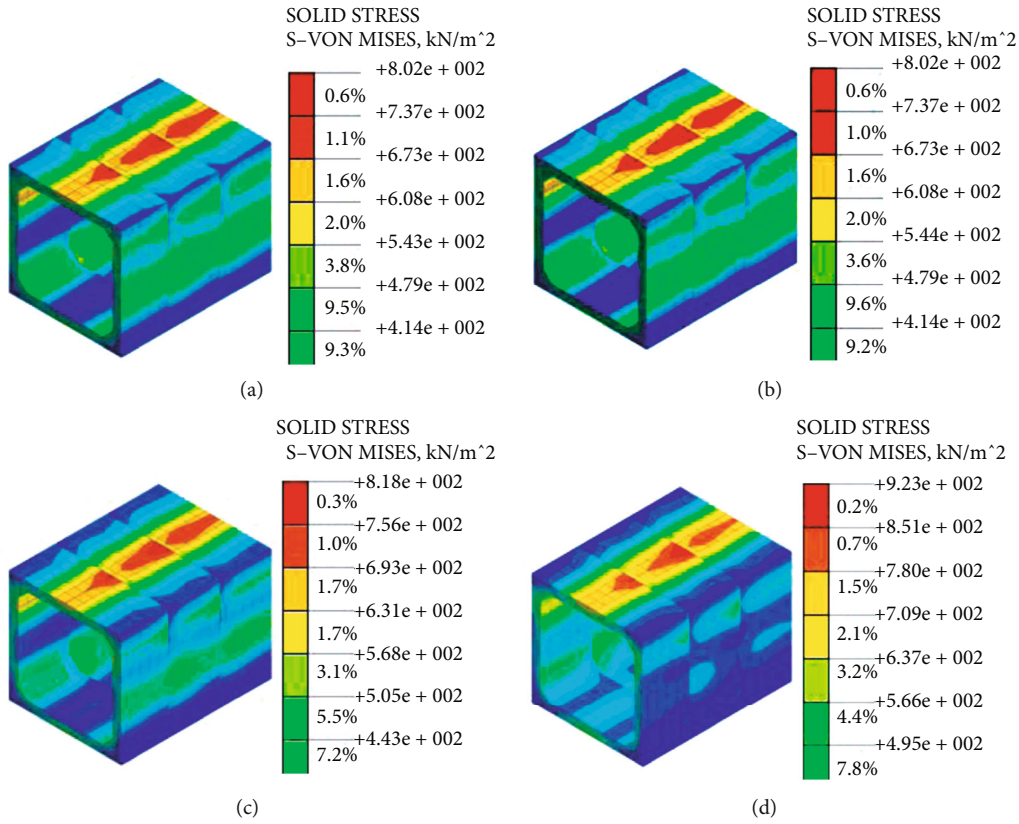

Figure 13: The overall Mises stress cloud map of the integrated pipe gallery under different groundwater levels. (a) When the water level is at d4. (b) Rises from d4 to d3. (c) Rises from d3 to d2. (d) Rises from d2 to d1.

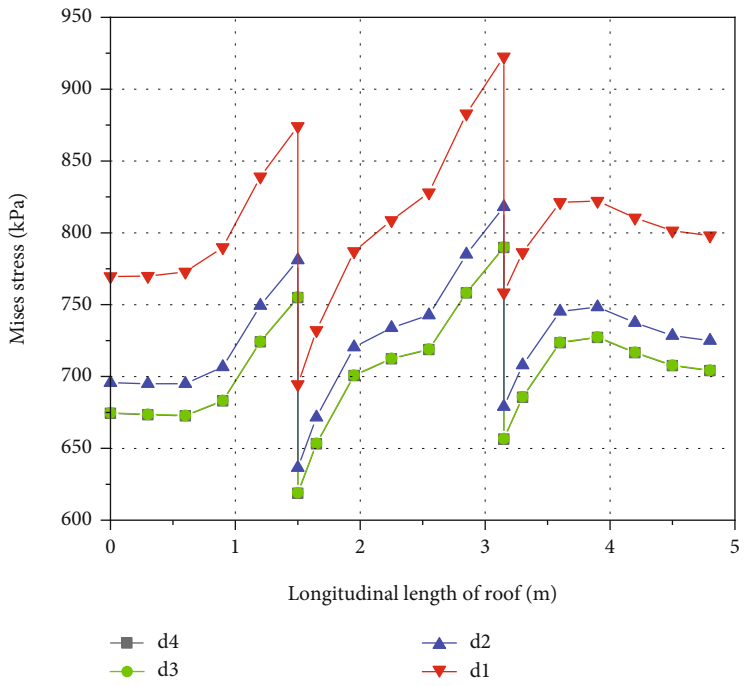

Figure 14: Longitudinal distribution curve of Mises stress on roof of integrated pipe gallery.

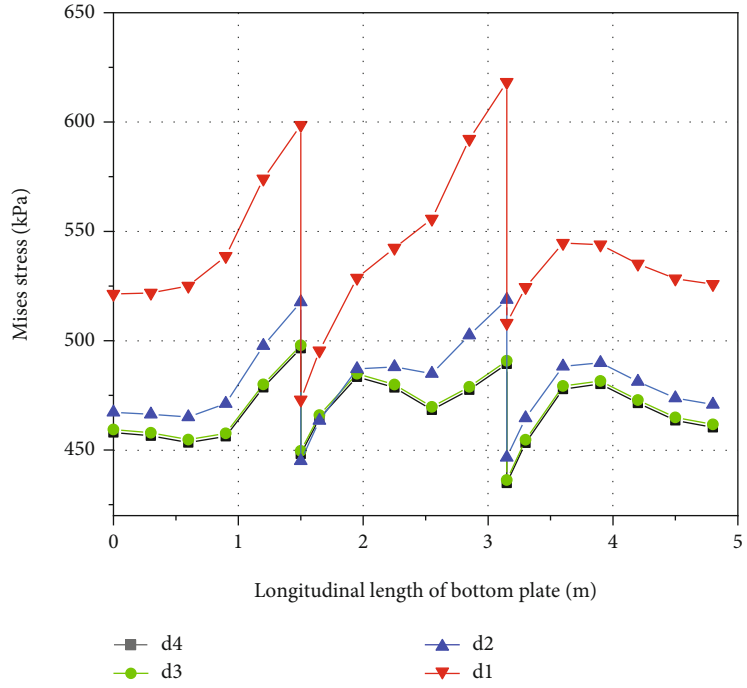

Figure 15: Longitudinal distribution curve of Mises stress on the bottom plate of integrated pipe gallery.

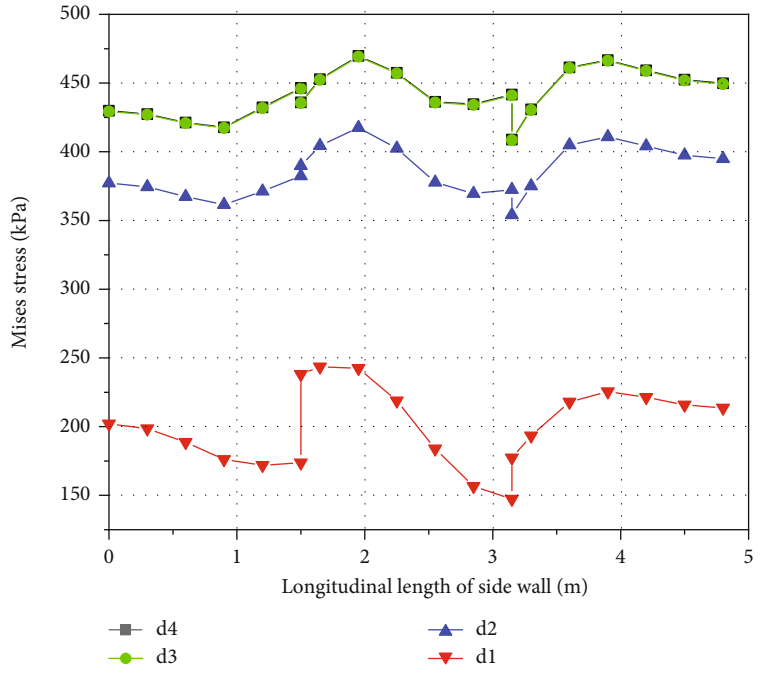

Figure 16: Longitudinal distribution curve of Mises stress on side wall of integrated pipe gallery.

4.2.2. Longitudinal Force Analysis of Integrated Pipe Gallery. According to Figures 13–16, with the increase of groundwater level, the peak values of Mises stress in pipe gallery roof are 789.75 kPa, 790.03 kPa, 818.12 kPa, and 922.62 kPa, respectively. The peak values of Mises stress in floor are 496.52 kPa, 497.88 kPa, 518.82 kPa, and 618.22 kPa, respectively. The peak values of Mises stress in sidewall are 469.71 kPa, 469.27 kPa, 417.51 kPa, and 243.57 kPa, respectively. The Mises stress peak value of the overall model of the pipe gallery is located at the joint of J_{2-3}, and the Mises stress peak value of the middle section of the pipe gallery is located on the N side of the joint; the Mises stress distribution curve of each part of the pipe gallery is not symmetrical along the center line of the coordinate axis; that is, there is

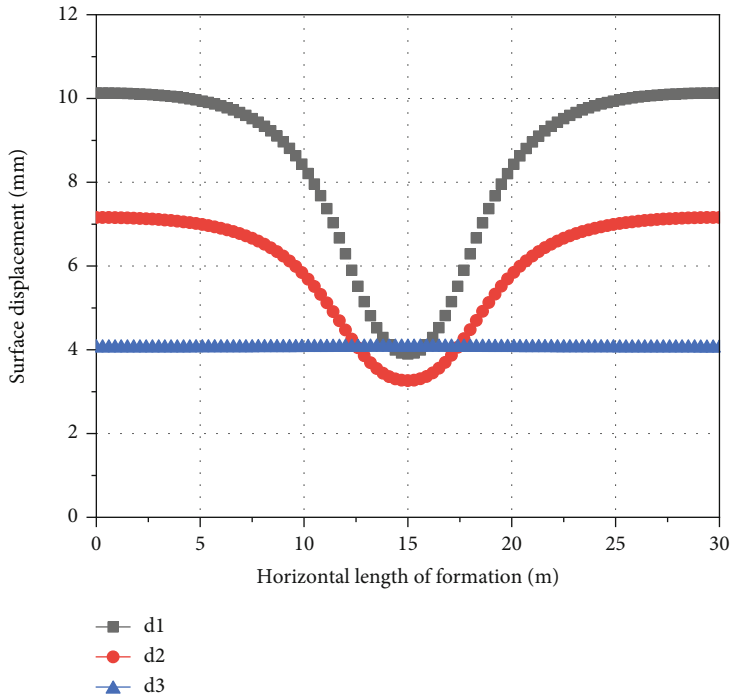

Figure 17: Effect of rising groundwater level on surface displacement.

an asymmetrical change trend with respect to the center of the overall model.

The change trend of the Mises stress value at the joints of the pipe gallery structure is not continuous, especially in the abscissa 1.5 m and 3.0 m, where the stress abrupt value appears; that is, the stress values at the joints J_{1-2} and J_{2-3} of the pipe gallery model are not continuous. The abrupt change value of stress showed a gradually increasing trend with the rise of groundwater level. It is especially noted that with the decrease of groundwater burial depth, the Mises stress of the side wall gradually decreases; so, the rise of groundwater level is beneficial to the side wall of the pipe gallery in the short-term.

4.2.3. Surface Displacement Change. It can be seen from Figure 17 that the surface displacement increases continuously with the rise of the groundwater level. When the water level rises to d3, the surface within the horizontal length of the stratum is uplifted by 4.0 mm. When the water level rises to d2 and d1, the surface displacement presents a "concave" type uplift, and the surface uplift displacement on both sides of the pipe gallery structure is basically the same. Due to the reduction of the effective stress, the surface uplift within the span of the pipe gallery is smaller than that on both sides of the pipe gallery structure.

4.2.4. Changes in Water Pressure. As shown in Figure 18, the rise of groundwater level has a greater impact on water pressure. With the continuous increase of soil burial depth, the water pressure shows a linear increase trend. Under the same soil burial depth, the higher the groundwater level, the higher the water pressure.

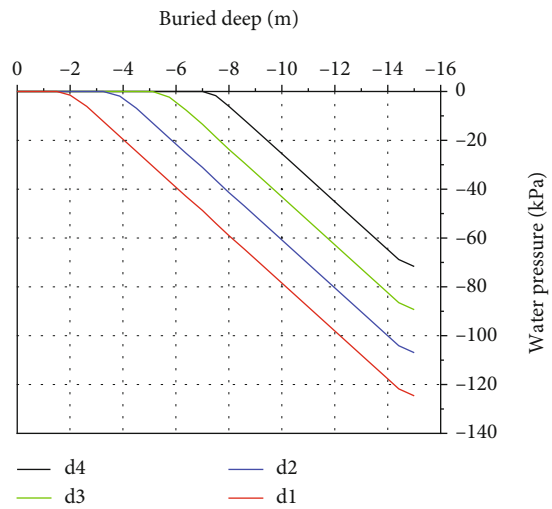

Figure 18: Effect of rising groundwater level on water pressure.

5. Engineering Examples

According to Figures 19, when the groundwater table depth is 3.8 m (in the middle of the side wall), the groundwater in the joint of the bottom plate of the pipe gallery is poured into the column, and the rubber waterproof belt is bounced out. The opening and dislocation of the joint will also lead to the friction between the sealing pad or between the sealing pad, and the cushion groove is less than the water pressure; so, the leakage occurs, and the operation of the pipe gallery is safe. The leakage at the socket will inevitably lead to the aging of the rubber gasket, the cracks and damage of the concrete at the junction, and the corrosion of the internal

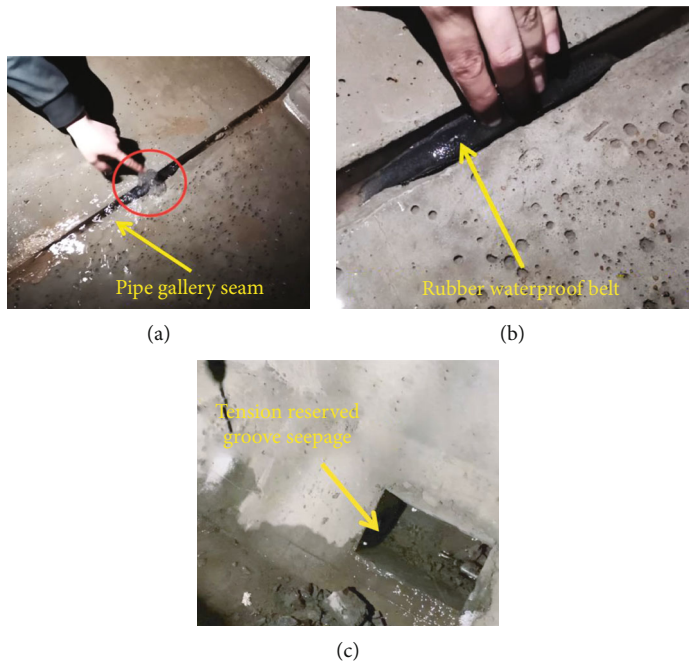

Figure 19: Serious water seepage in the integrated pipe gallery. (a) Water leakage at joints of integrated pipe gallery. (b) The rubber waterproof belt is bounced out. (c) Serious water seepage in the reserved groove for the tensioning of the pipe gallery.

equipment of the pipe gallery. These conditions will reduce the service life of the pipe gallery; so, the influence of groundwater on the pipe gallery cannot be ignored.

Since the change of the groundwater level will have a certain degree of influence on the underground structure, the function of the structure may be greatly affected within the designed service life. If the underground structure is damaged within the designed service life, certain preventive measures should be taken to prevent the change of the groundwater level.

6. Discussion

When many researchers study the problem of groundwater level rise, they mostly study from the perspective of a factor that causes damage to underground structures after the rise of the groundwater level. The reason for the damage to structures after the rise of the groundwater level is not only due to one aspect. However, there are several aspects that comprehensively affect the underground structure. One of the main influencing factors is that after the groundwater level rises, it will produce certain water buoyancy and hydrostatic pressure on the foundation of the underground structure or above-ground structure. On the other hand, after the groundwater level rises, the surrounding rock and soil parameters around the underground structure are weakened, and the weakening of the surrounding rock of the soil layer in turn has a certain impact on the underground structure. There may be certain corrosive ions in the groundwater. After the level rises, the underground structure may be corroded and damaged in the long-term immersion in groundwater.

The rise of groundwater level will have a certain impact on the underground structure. For the urban integrated pipe gallery structure in different regions and different locations, due to the different formation conditions of the underground structure, the buried depth of the underground structure and other factors may also lead to different hazards of the same underground structure in the process of water level rise. Therefore, it is necessary to summarize the hazards of the integrated pipe gallery structure under different buried depths in the process of water level rise and analyze the causes of the hazards.

7. Conclusion

The following conclusions were drawn based on this study:

(1) When the buried depth of the groundwater level is the same, for the stress change trend of the cross-section of the integrated pipe gallery, the analysis of the test results is basically consistent with the numerical simulation calculation results. The test data verifies the validity of the numerical simulation calculation and has reference value

(2) The Mises stress on the roof and bottom of the integrated pipe gallery increases continuously with the rise of the groundwater level. Due to the effect of the effective stress, the Mises stress on the side wall shows a decreasing trend

(3) Due to the influence of the construction form of the cross-section interface, the maximum principal stress of each part of the M side is always smaller than that of the N side; with the continuous increase

of groundwater level, the maximum principal stress at each part of the N and M sides of the pipe gallery structure joint gradually increases

(4) The overall structure of the pipe gallery floats up, and the bottom plate moves upward due to the action of the buoyancy force. However, when the water level tends to be stable, due to the effect of the self-weight of the integrated pipe gallery structure itself and the effect of the effective stress, the entire structure will have a certain degree of displacement. In the degree of subsidence, the surface displacement is rising with the rise of the groundwater level

(5) The engineering example shows that the impact of groundwater on the integrated pipe gallery cannot be ignored to reduce the service life of the integrated pipe gallery

Data Availability

The data used to support the findings of this study are available from the corresponding author upon request.

Conflicts of Interest

The authors declare that there is no conflict of interest regarding the publication of this paper.

Acknowledgments

This research was funded by the National Natural Science Foundation of China (NSFC), grant number 51778351.

References

[1] H. T. Wang, L. G. Wang, S. C. Li, Q. Wang, P. Liu, and X. J. Li, "Roof collapse mechanisms for a shallow tunnel in two-layer rock strata incorporating the influence of groundwater," *Engineering Failure Analysis*, vol. 98, pp. 215–227, 2019.

[2] B. Wu, W. Huang, Z. Deng, Z. Zhang, J. Xu, and H. Chen, "Stability analysis of metro shield construction in sandy soil strata under tidal forces in coastal areas," *Journal of Coastal Research*, vol. 37, no. 5, pp. 946–952, 2021.

[3] X. W. Tang, P. L. Gan, W. Liu, and Y. Zhao, "Surface settlements induced by tunneling in permeable strata: a case history of Shenzhen Metro," *Journal of Zhejiang University-Science A*, vol. 18, no. 10, pp. 757–775, 2017.

[4] Y. J. Shin, D. H. Kim, and I. M. Lee, "Numerical simulation of seepage-induced behavior of tunnel for analyzing deformation characteristic and estimating geotechnical parameters," *KSCE Journal of Civil Engineering*, vol. 18, no. 2, pp. 659–671, 2014.

[5] J. C. Xu and N. Li, "Influence of continuous rainfall on surrounding rock-initial support system of shallow decomposed-rock tunnel," *Environmental Earth Sciences*, vol. 61, no. 8, pp. 1751–1759, 2010.

[6] P. Bhattacharya and P. Dutta, "Stability of rectangular tunnel in Hoek–Brown rocks under steady-state groundwater flow," *Geotechnique Letters*, vol. 10, no. 4, pp. 524–534, 2020.

[7] S. C. Li, C. Xie, Y. H. Liang, and Q. Yan, "Seepage flow model and deformation properties of coastal deep foundation pit under tidal influence," *Mathematical Problems in Engineering*, vol. 2018, Article ID 9714901, 10 pages, 2018.

[8] X. H. Deng, Y. C. Wang, R. Wang, D. Xia, and Z. Zhao, "Application of modified Hoek–Brown strength criterion in water-rich soft rock tunnel," *Geofluids*, vol. 2021, Article ID 5552791, 12 pages, 2021.

[9] Y. C. Wang, Y. Liu, Y. L. Li, W. Jiang, and Y. Wang, "Experimental study on the failure mechanism of tunnel surrounding rock under different groundwater seepage paths," *Geofluids*, vol. 2021, Article ID 8856365, 17 pages, 2021.

[10] Z. D. Wei and Y. P. Zhu, "Seepage in water-rich loess tunnel excavating process and grouting control effect," *Geofluids*, vol. 2021, Article ID 5597845, 13 pages, 2021.

[11] Q. N. Guo, J. W. Huang, Z. F. Zhou, and J. Wang, "Experiment and numerical simulation of seawater intrusion under the influences of tidal fluctuation and groundwater exploitation in coastal multilayered aquifers," *Geofluids*, vol. 2019, Article ID 2316271, 17 pages, 2019.

[12] Z. J. Hu, Q. B. Wang, S. Yang et al., "Numerical simulation of soil displacement and settlement in deep foundation pit excavations near water," *Geofluids*, vol. 2021, Article ID 5559009, 14 pages, 2021.

[13] T. L. Gia, L. T. Duy, T. D. T. Kieu, and H. N. Thu, "The impact of groundwater lowering on pile bearing capacity in Hanoi – Vietnam," *Geotechnics for Sustainable Infrastructure Development*, vol. 62, pp. 137–144, 2020.

[14] Y. Roh, I. Kim, G. Kim, and J. Lee, "Comparative analysis of axial load capacity for piled-raft foundation with changes in groundwater level," *KSCE Journal of Civil Engineering*, vol. 23, no. 10, pp. 4250–4258, 2019.

[15] K. Saowiang and P. H. Giao, "Numerical analysis of subsurface deformation induced by groundwater level changes in the Bangkok aquifer system," *Acta Geotechnica*, vol. 16, no. 4, pp. 1265–1279, 2021.

[16] C. H. Shi, C. Y. Cao, M. F. Lei, and W. Yang, "Face stability analysis of shallow underwater tunnels in fractured zones," *Arabian Journal of Geosciences*, vol. 9, no. 1, 2016.

[17] B. Zhang, H. X. Wang, Y. W. Ye, J. L. Tao, L. Z. Zhang, and L. Shi, "Potential hazards to a tunnel caused by adjacent reservoir impoundment," *Bulletin of Engineering Geology and the Environment*, vol. 78, no. 1, pp. 397–415, 2019.

[18] X. Ding, Y. Zhang, Q. Wu, G. Cao, and Z. Chen, "Effects of groundwater level on the seismic responses of coral sand ground and superstructure by shaking table tests," *Acta Geotechnica*, vol. 17, no. 7, pp. 3047–3066, 2022.

[19] L. Ratnika, L. Gaile, and N. I. Vatin, "Impact of groundwater level change on natural frequencies of RC buildings," *Buildings*, vol. 11, no. 7, p. 265, 2021.

[20] J. Shi, B. Wu, Y. Liu et al., "Analysis of the influence of groundwater seepage on the deformation of deep foundation pit with suspended impervious curtain," *Advances in Mechanical Engineering*, vol. 14, no. 3, Article ID 16878132221085128, 2022.

[21] C. Wu, X. Wu, C. Y. Lu et al., "Characteristics and driving factors of lake level variations by climatic factors and groundwater level," *Journal of Hydrology*, vol. 608, article 127654, 2022.

[22] C. F. Zeng, S. Wang, X. L. Xue, G. Zheng, and G. X. Mei, "Characteristics of ground settlement due to combined actions of groundwater drawdown and enclosure wall movement," *Acta Geotechnica*, pp. 1–18, 2022.

[23] A. Zaryab, H. R. Nassery, and F. Alijani, "The effects of urbanization on the groundwater system of the Kabul shallow aquifers, Afghanistan," *Hydrogeology Journal*, vol. 30, no. 2, pp. 429–443, 2022.

[24] P. P. Zhou, G. C. Wang, and R. Q. Duan, "Impacts of long-term climate change on the groundwater flow dynamics in a regional groundwater system: case modeling study in Alashan, China," *Journal of Hydrology*, vol. 590, article 125557, 2020.

[25] Q. Liu, L. Q. Liang, X. M. Yuan, X. Mou, and L. Su, "Effects of groundwater level changes associated with coastline changes in coastal wetlands," *Wetlands*, vol. 40, no. 5, pp. 1647–1656, 2020.

[26] B. Z. Yan, X. M. Li, J. L. Hou, P. Bi, and F. Sun, "Study on the dynamic characteristics of shallow groundwater level under the influence of climate change and human activities in Cangzhou, China," *Water Supply*, vol. 21, no. 2, pp. 797–814, 2021.

[27] F. Q. Guo, G. T. Li, and M. J. Cheng, "An analysis of the influences of groundwater level changes on the frost heave and mechanical properties of trapezoidal channels," *Water Policy*, vol. 22, no. 6, pp. 1163–1181, 2020.

[28] H. J. Chen, X. J. Li, W. M. Yan, S. Chen, and X. Zhang, "Shaking table test of immersed tunnel considering the geological condition," *Engineering Geology*, vol. 227, pp. 93–107, 2017.

[29] Y. Li, H. P. Wang, W. S. Zhu, S. Li, and J. Liu, "Structural stability monitoring of a physical model test on an underground cavern group during deep excavations using FBG sensors," *Sensors*, vol. 15, no. 9, pp. 21696–21709, 2015.

[30] Q. H. Chai, Z. K. Li, J. Wang, Z. Ding, and M. Jiao, "Similar materials and engineering application of cemented sand and gravel dam model," *Advances in Civil Engineering*, vol. 2020, Article ID 8887112, 10 pages, 2020.

[31] J. Shi and D. S. Kong, "Floor heave mechanism and anti-slide piles control technology in deep and large-span chamber," *Applied Sciences-Basel*, vol. 11, no. 10, 2021.

[32] J. Chai, W. Du, Q. Yuan, and D. Zhang, "Analysis of test method for physical model test of mining based on optical fiber sensing technology detection," *Optical Fiber Technology*, vol. 48, pp. 84–94, 2019.

[33] X. L. Jiang, F. F. Wang, H. Yang et al., "Dynamic response of shallow-buried tunnels under asymmetrical pressure distributions," *Journal of Testing and Evaluation*, vol. 46, no. 4, pp. 1574–1590, 2018.

[34] Y. Zhao, Z. Cheng, Y. Gao, S. Wu, and C. Chen, "Review of geomechanical similar-material test systems," *Arabian Journal of Geosciences*, vol. 13, no. 18, p. 906, 2020.

[35] H. Chen and W. Z. Ren, "Development of epoxy-silicone rubber-based geotechnical similar material and its engineering application," *Materials Research Innovations*, vol. 19, Supplement 5, pp. S5–S296, 2015.

[36] Y. Zhao and L. He, "Nonlinear progressive failure analysis of surrounding rock system based on similarity theory," *MATEC Web of Conferences*, vol. 64, 2016.

[37] L. Dong, J. Cao, and X. Liu, "Risk control method and practice in the whole construction process of a shield tunneling pipe gallery in complex surrounding underground environment," *ASCE-ASME Journal of Risk and Uncertainty in Engineering Systems, Part A: Civil Engineering*, vol. 8, no. 3, 2022.

[38] H. Y. Zhao, P. J. Ming, W. P. Zhang, Q. Liu, and W. L. Qi, "Three-dimensional simulation of two-phase flow in a complex gallery and telescopic pipe coupled system," *Applied Thermal Engineering*, vol. 169, article 114918, 2020.